Design and Flight Test Evaluation of a Laminar Wing Glove on a Commuter Aircraft

W. Wohlrath, H. Echtle, P. Dick, D. Welte, H.W.-Stock, B. Moeken
Dornier Luftfahrt GmbH, Aerodynamics-Dept., D-88039 Friedrichshafen

K.H. Horstmann, R. Müller, C.-H. Rohardt, A. Quast
Deutsche Forschungsanstalt für Luft- und Raumfahrt e.V. (DLR)
Institute of Design Aerodynamics, Postfach 3267, D-38022 Braunschweig

Abstract

As part of a joint venture between DASA/Dornier Luftfahrt GmbH and DLR Braunschweig, a laminar wing glove was designed for the Do 228 turboprop aircraft. The glove, covering nearly 50 % of half-span, was attached to the right wing of the aircraft.

The extensive flight tests, performed in close cooperation between DLR and DORNIER, included the evaluation of the laminar properties in the undisturbed glove region and in the propeller slipstream region. The influence of disturbances due to simulated surface imperfections was studied to determine the magnitudes for allowable manufacturing tolerances. A liquid cleaning and de-icing system covering a spanwise region of 1 m was tested on the outer part of the glove.

In this paper, some of the design aspects of the glove are discussed and the main results of the flight test are presented.

1. Introduction

Research programs have shown that laminar flow can be maintained on wings with moderate sweep for chord Reynolds numbers in the range of 12 to 16 million using natural laminar flow (NLF). By shaping the airfoil to have favorable upper and lower surface pressure gradients, laminar runs of up to 60 % chord-length on commercial airplanes are possible.

To get insight into the problems associated with the application of NLF-technology to commuter type aircraft, in this case the Do 228 shown in **Fig. 1**, a research program was initiated which addressed the following items:

- Verification and improvement of the design tools (transition prediction) for NLF airfoils.
- Verification of an NLF-airfoil in flight.
- Test and improvement of a fluidic anti-contamination and de-icing system.
- Investigation of the propeller slipstream region and determination of the drag reduction caused by laminar effects.
- Test of the influence of disturbances representing surface imperfections to determine the magnitude and kinds of allowable manufacturing tolerances.

2. Glove design

2.1 Wing geometry and geometrical constraints

In **Fig. 2** the glove and wing geometry are shown. The glove covers 45 % of half-span, which corresponds to 3.5 m in actual span. In order to keep the landing flap and aileron unchanged, the surface was allowed to be modified only up to 75 % chord on the upper and 65 % on the lower surface. To allow for the wiring of the measuring equipment, a minimum glove thickness of 7 - 10 mm was required [1].

2.2 Aerodynamic requirements

2.2.1 Requirements for airfoil design

At the design point, the Reynolds number based on the mean aerodynamic chord is 13 million. For Reynolds numbers in this range, accelerated flow must exist up to the desired transition point. For this reason, the required amount of laminar flow of 60 % also determines the position of the start of the main pressure recovery.

For a c_L value, corresponding to the climb condition, no trailing edge separation is allowed.

The maximum lift coefficient of the NLF airfoils should be comparable to the values of the turbulent airfoils. Because the required acceleration results in a thinner leading edge for the NLF airfoils, a careful design of the nose region is important.

2.2.2 Requirements for three-dimensional glove design

In order to keep the additional rolling moment caused by the glove as small as possible, the spanwise load distribution had to be maintained.

To be certain that the results obtained in the different spanwise regions were comparable, no change in the baundary layer in spanwise direction was allowed. This means that the N-factor had to be kept constant on percent lines of airfoil chord. The N-factor is a measure for transition loca-

tion using boundary-layer stability theory.

In the propeller slipstream region, it was required that the pressure distributions altered by the propeller swirl must allow laminar flow.

2.3 Aerodynamic properties of the inner and outer glove section

To achieve the desired aerodynamic properties of the glove, airfoils had to be designed for both the inner and outer span stations. In **Fig. 3** the calculated properties of the inner glove section at Re_c = 14.8 million are shown. On the left, the drag polars for free and fixed transition (5 %) are presented. Within the laminar bucket, the transition is approximately at x/c = 55 % on both the upper and lower surfaces.

With the definition of the bucket form (bucket width and upper and lower c_L limits) for the inner airfoil, the corresponding values for the outer airfoil are determined by the spanwise wing lift distribution (**Fig. 4**).

2.4 Propeller region

The qualitative behaviour of a laminar baundary layer influenced by a propeller slipstream is already known from flight and wind-tunnel investigations [2]. Under certain conditions, laminar flow is not totally lost in a slipstream affected region. Hot-film signals in this region show an alternating laminar/turbulent behaviour of the boundary-layer. The turbulent part of the signal is caused by the viscous propeller-blade wake.

Besides this viscous effect within the baundary layer, the propeller swirl has an influence on the wing pressure distribution. This change in pressure distribution must be known for the design of the inner glove airfoil. Therefore the propeller influence was calculated with a panel method. In **Fig. 5,** the result of this calculation is presented. The influence of the propeller swirl reduces the acceleration in the wing region behind the upward moving blade. The adverse effect on boundary-layer stability (N-factor) is shown in **Fig. 6**. To achieve the desired N-envelope, the airfoil in the propeller region had to be designed with higher accelerations on the upper surface.

3. Test equipment

In Fig. 1 the Do 228 test aircraft with the additional test-equipment, i.e., the laminar glove on the right wing, a flightlog on the noseboom, a movable wake-rake system, and the pod with mounting system for the infrared camera, is shown.

The laminar glove with the main dimensions is shown in **Fig. 7**. The glove covers the whole outer wing except for the triangular tip region. It is made of glass-fibre and contains two rows of pressure taps on both the upper and lower surfaces. One row is in the propeller region at r/R = 0.85, the second in the middle part of the glove. Each row has 60 static pressure taps. Two hot-film arrays, each having eight films, are located behind the propeller on the upper and lower surface in the position at r/R = 0.67.

The outer one third of the glove contains a fluidic contamination protection system in the leading edge, which also can be used as an anti-ice-system. Observation of the boundary-layer conditions of the glove surface is done by two infrared cameras. The upper camera is mounted in a pod 2.2 m over the wing using a four-legged support system. To observe the lower glove surface, a camera is located in the right main landing-gear box. To generate different temperatures between the glove surface and the freestream (necessary for the infrared observation), the surface can be heated [3]. The heating is controlled automatically by eight temperature sensors.

The drag of different glove sections can be measured by a rake system having 70 total- and five static-pressure probes. The rake can be moved in the spanwise direction during flight over a distance of 0.52 m. By changing the rake position before flight on the support tube, the drag behind either the propeller or the undisturbished section can be measured.

To get the angle of attack and yaw, a flightlog mounted on a noseboom 1.7 m in front of the fuselage was used. All required pressures (total, static, calibration) are measured using high precision pressure sensors. The flight measurements were taken with a self-contained data acquisition and reduction system with quick-look capability for evaluating the results directly during flight.

Fig. 8 shows an example of an infrared image from the glove upper side in cruise flight conditions. The laminar baundary layer is marked by the white field, which reaches up to 55 % chord. A turbulent wedge, caused by the holes of the pressure tap row, can be observed to run from the leading edge.

4. Results

4.1 Drag of the laminar profile

The measured polar of the laminar profile in the undisturbed middle part of the glove is shown in **Fig. 9**. The very small scatter of the measured drag values, which were taken in four different flights, is notable. The polar shows a very distinct laminar drag bucket with a minimum drag coefficient of c_D = 0.0037 at a Reynolds number of 15 million.

Fixing the transition at 5 % chord on both upper and lower surface causes the drag to be nearly doubled (**Fig. 10**). For these measurements, the thickness of the zig-zag shaped transition strip was optimized by controlling the transition location using the infrared image capability.

To determine the influence of the engine- and propeller noise on the laminar-turbulent transition, drag measure-

ments with the right engine not running were made. As shown in **Fig. 11**, the drag is quite the same with and without the engine operating. The differences are within the accuracy of the measurements. It is concluded that the noise of the engine-propeller system has no measurable influence to the transition location.

4.2 Drag behind the propeller

Turboprop driven regional airliners have a relatively large amount of the wing in the propeller slipstream. To ascertain the penalty of losing laminar drag in this region, hot-film measurements at the station r/R = 0.67 were made [4]. **Fig. 12** shows the hot-film signals obtained with the two arrays. On the lower side, two films were damaged and not operating.

One can see the time history of the boundary-layer condition during one rotation of the propeller at different chord positions (left scale), and the percentage of laminar flow time at these positions (right scale). Outside of the propeller slipstream region, natural transition occurs at 55 % chord. This is considered 100 % laminar flow benefit. Evaluation of the data taken in the slipstream indicate that, on the upper surface, 30 % of the drag benefit obtained with natural transition is achieved, while on the lower side, a benefit of 32 %. Similar results were found by measuring the wake drag behind the propeller. The wake measurements in this region are complicated, however, by the fact that the total pressure in the slipstream is not unique, and it is somewhat difficult to define the actual wake region.

Fig. 13 contains the measured drag behind the propeller. It is shown that there is an advantage of using laminar profiles in the propeller slipstream region relative to having conventional turbulent airfoils there.

4.3 Influence of surface disturbances

To achieve laminar flow at Reynolds numbers of 15 million, it is necessary to have an undisturbed surface. For manufacture, it is important to know what type and height of disturbances can be tolerated for a laminar wing. Therefore, extensive investigations were carried out with simulated rivet heads, forward- and rearward-facing steps, and inspection hole covers with different heights and chord positions.

Fig. 14 shows, for example, the infrared image of rivet heads located at different chord positions from 3 to 25 percent. In this region, all rivet heads with a height of 6 h, where h is a proprietary quantity, disturb the flow and turbulent wedges are observed. As shown in **Fig. 15**, the influence of these three-dimensional disturbances to the laminar-turbulent transition depends on the height and the location. Heads with h = 1 and located behind 20 % chord have no influence on laminar flow and are tolerable.

The sensitivity of the boundary-layer stability to three-dimensional disturbances is much greater than it is to two-dimensional ones, such as forward- and rearward-facing steps. Such steps result by fitting, for example, a nosepart to the main wingbox. In **Fig. 16**, the infrared image of a forward-facing step with the height of 6 h running from 5 to 25 percent chord show that such steps do not disturb the baundary layer behind 10 % chord. The results for different step heights are shown in **Fig. 17**. Forward-facing steps of a height below 4 h do not disturb the flow at any location, including the immediate leading edge region.

The boundary-layer stability is more sensitive to rearward-facing steps than it is to forward-faci ones.

4.4 Anti-contamination system

To achieve the full low drag potential of a laminar wing, it is essential that the wing surface and, especially the leading edge, is kept clean. Flight in the thermal convection layer, such as during take off, climb, descent and landing, can result in leading edge contamination by insects. The amount of contamination depends mainly on factors such as temperature, wind velocity and, most important, local geographical conditions. In Mid-Europe, especially in the months June and July, insect contamination can be great. **Fig. 18** demonstrates the influence of insect contamination on the drag polar during three different flights. The drag values of the different flights are more or less the same. They are nearly as high as those of a turbulent baundary layer tripped at 5 % of chord length, as indicated by the dashed line. The benefit of laminar flow is nearly lost.

One possibility to avoid the insect contamination is to apply a fluid film on the leading edge surface. The fluid film reduces the adhesive forces by orders of magnitude. The insects stick much less on the surface and are removed downstream by means of the fluid layer and the shear stress of the flow.

The special advantage of such a fluidic anti-contamination system is the possibility of combining this system with a fluidic anti-icing system [5]. The wing leading edge region is equipped with a porous surface consisting of a laser drilled titanium sheet with typical hole-diameters of 50 microns and a spacing of 0.5-1.0 mm. A mixture of glycol alcohol and water is pressed through the porous surface forming a closed film while the fluid is moved downstream by the flow shear stresses. Such an anti-contamination system must fulfill some important conditions:

- The system must not disturb the laminar baundary layer when not operating.
- In the active phase, a sufficient surface wetting is necessary to form a closed fluid film. This can be achieved by controlling the mass-flow through the panel and adding a wetting agent to the fluid.
- When the glycol flow is switched off, a fast and complete relaminarization of the flow must be achieved.

During three flight-test periods and four wind-tunnel test periods, different anti-contamination systems and their

modifications were tested. For the flight tests, a cleaning panel with a spanwise length of one meter was installed in the outer part of the Do 228 glove. The central zone of the glove was taken as reference. The glove surface was painted using polyester resin.

Fig. 19 shows a typical upper side infrared image of a contamination flight test. In the outer part of the glove, protected by the anti-contamination system, the boundary-layer remains laminar except for a single turbulent wedge. The reference zone in the central part of the image is, on the other hand, characterized by many turbulent wedges. Downstream of 10 % chord only some small laminar regions are left.

This amount of contamination was achieved during six take offs and landings The effectiveness of the anti-contamination system can be defined by comparing the number of wedges in the cleaning zone to those in the reference zone. Typically in the cleaning zone, only 10 % of the insects stick as compared to in the reference zone.

Summarizing, the tests show that a fluidic anti-icing system with some modifications can successfully be used as an anti-contamination system of a laminar wing. There still exist some difficulties, however, especially in the uniform wetting of the surface and a fast and complete relaminarization after switching off the system.

5. Comparison of theoretical results with the flight measurements

The main objective of the glove design was to obtain laminar flow on more of half the surface in cruise flight conditions, and to achieve a drag coefficient on order of $c_D = 0.004$. On the other hand, it was not allowed to change the handling qualities of the basic Do 228 aircraft, especially in the low speed region.

A comparison of a calculated pressure distribution with a measured one is shown in **Fig . 20**. The agreement is very good, including the trailing edge pressure. Quite the same agreement was found by comparing the calculated and measured drag polars with natural and fixed transition, as shown in **Fig. 21**. The measured drag in the laminar bucket region corresponds well with the calculated values. Outside the bucket the measured drag is slightly higher. With transition fixed at 5 % on both the upper and lower surfaces, the measured drag coefficient is slightly lower than calculated. This may be caused by underfixing transition in the low-lift region, as the strip optimization was done for the lift of the upper edge of the laminar bucket.

6. Conclusions

The experience gained in this research program shows that NLF can be used for reduction of viscous drag in an operational environment typical of commuter aircraft.

The results of the wake measurements show that the reduction in profile drag is predicted correctly by the theoretical tools applied.

For undisturbed laminar flow (transition location x/c = 55 %), the reduction on profile drag in the glove region outside propeller slipstream is on the order of 50 % of the turbulent value (transition location x/c = 5 %).

A reduction in drag due to laminar effects also remains to some extent in the propeller slipstream region. The drag reduction in this region is about 14 % at the turbulent value.

The anti-contamination system tested reduces the number of insects adhering to the surface to 10 % of the number sticking in the reference region where no cleaning system is installed.

The influence of surface imperfections depends strongly on the geometry of the disturbance. Forward-facing steps can be tolerated within reasonable manufacturing tolerances, while rearward-facing steps cannot. For three-dimensional disturbances, like rivets, only a small region in the vicinity of the nose exists where they can be tolerated at all.

The flight tests with the laminar glove demonstrated no noticeable changes in the handling qualities over the whole speed range, including the stall.

Generally, all of the desired objectives for the glove were obtained in the flight measurements.

7. References

[1] W. Wohlrath, C.-H. Rohardt, K.H. Horstmann
The Laminar Glove on the Dornier 228 Wing-Design and First Results.
Vortrag 9201-049, First European Forum on Laminar Flow Technology, Hamburg, 16-18/3/1992.

[2] R.H. Howard, S.J. Miley, B.J. Holmes
An Investigation of the Effects of the Propeller Slipstream on the Laminar Boundary Layer.
SAE Paper 850859, 1985.

[3] A. Quast
Detection of Transition by Infrared Image Technique.
ICIASF'87 Record, 1987, pp. 125-133.

[4] B. Ewald, F. Durst, E. Krause, W. Nietsche
In Flight Measuring Techniques for Laminar Flow Wing Development.
DGLR/AAAF/RAeS Proceedings: First European Forum on Laminar Flow Technology.
DGLR-Bericht 92-06 (1992), pp. 110-122.

[5] B.E. Humphreys
Surface Contamination Avoidance for Laminar Flow Surfaces.
DGLR/AAAF/RAeS Proceedings: First European Forum on Laminar Flow Technology.
DGLR-Bericht 92-06 (1992), pp. 262-269.

Fig. 1 Do 228 test aircraft with right wing laminar glove

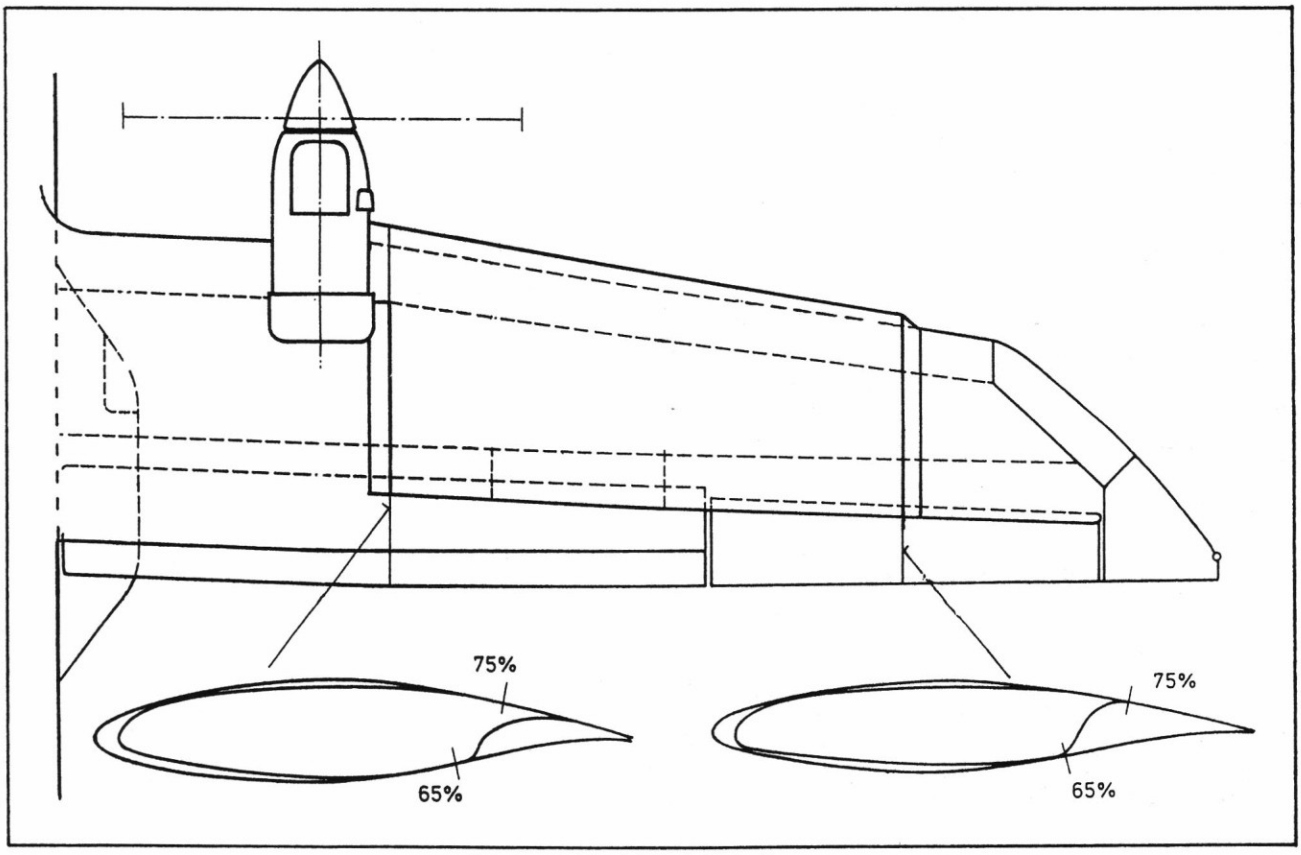

Fig. 2 Glove and wing geometry overview

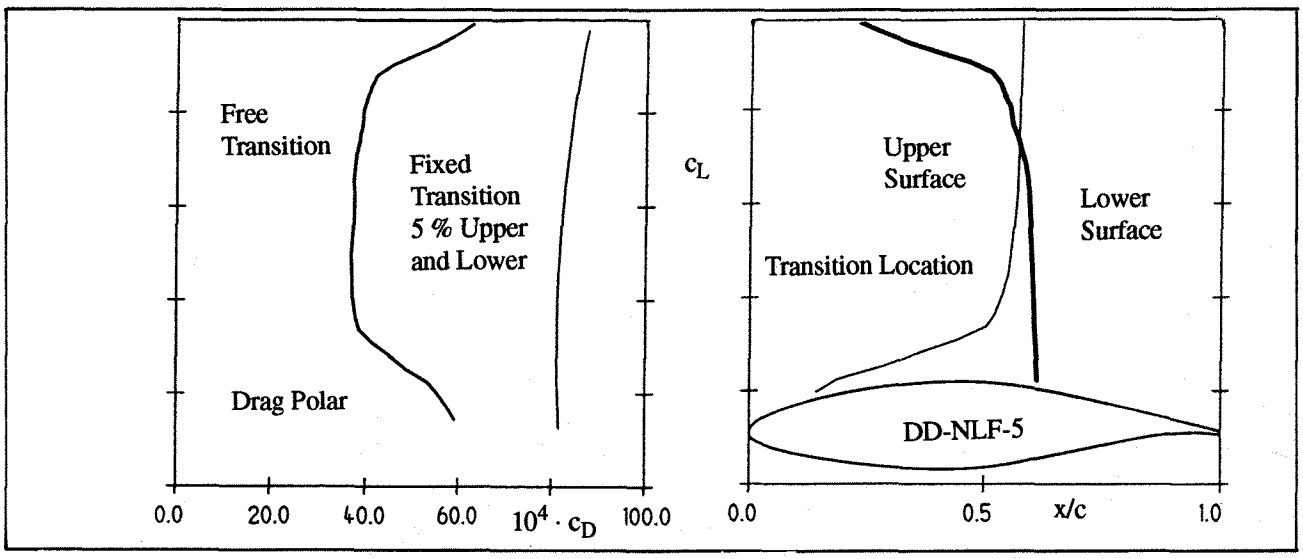

Fig. 3 Calculated aerodynamic properties of the inner glove section

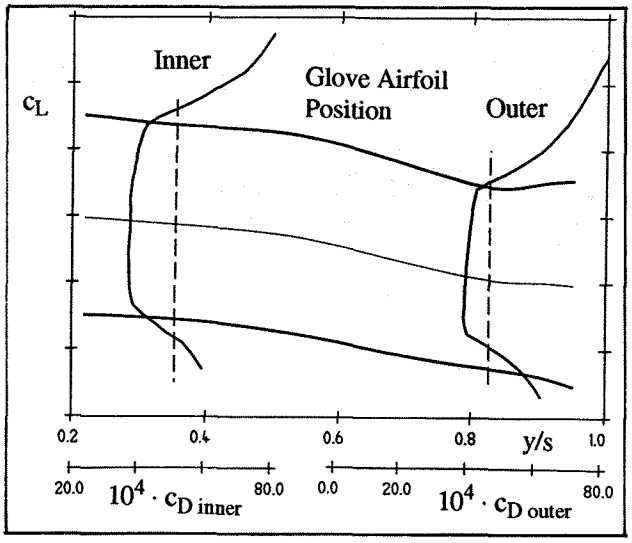

Fig. 4 Spanwise liftdistribution and polars of the inner and outer airfoil

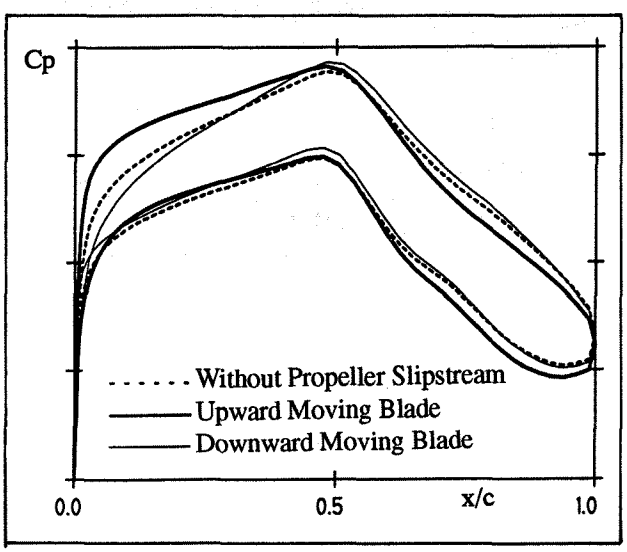

Fig. 5 Calculated propeller influence on the chordwise pressure distribution

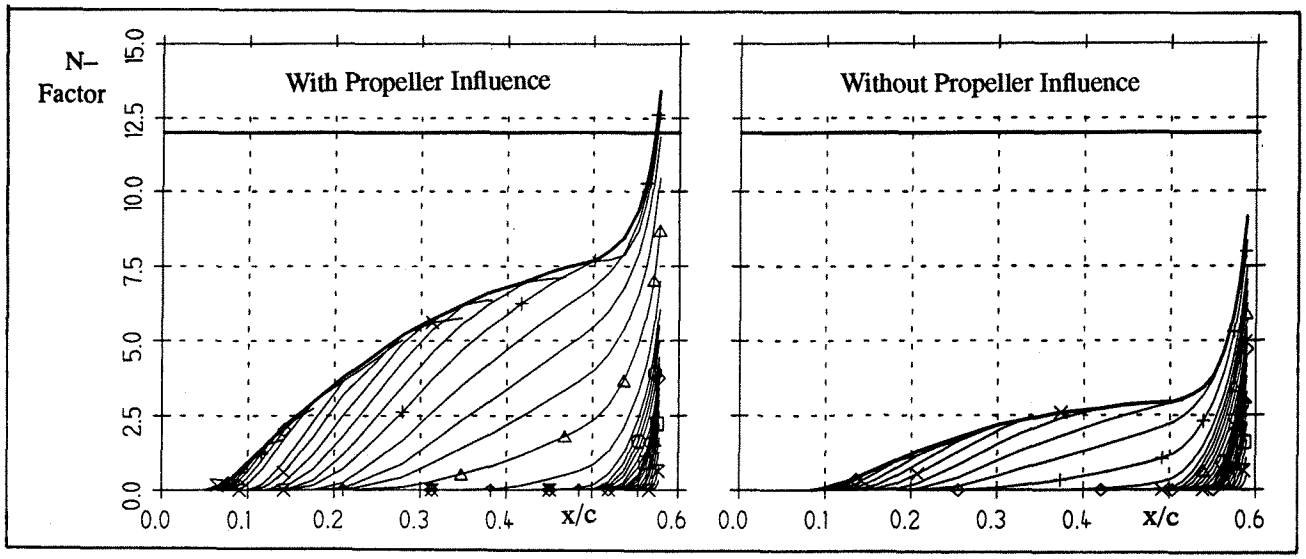

Fig. 6 Comparison of the local N-factor on the upper surface (design point)

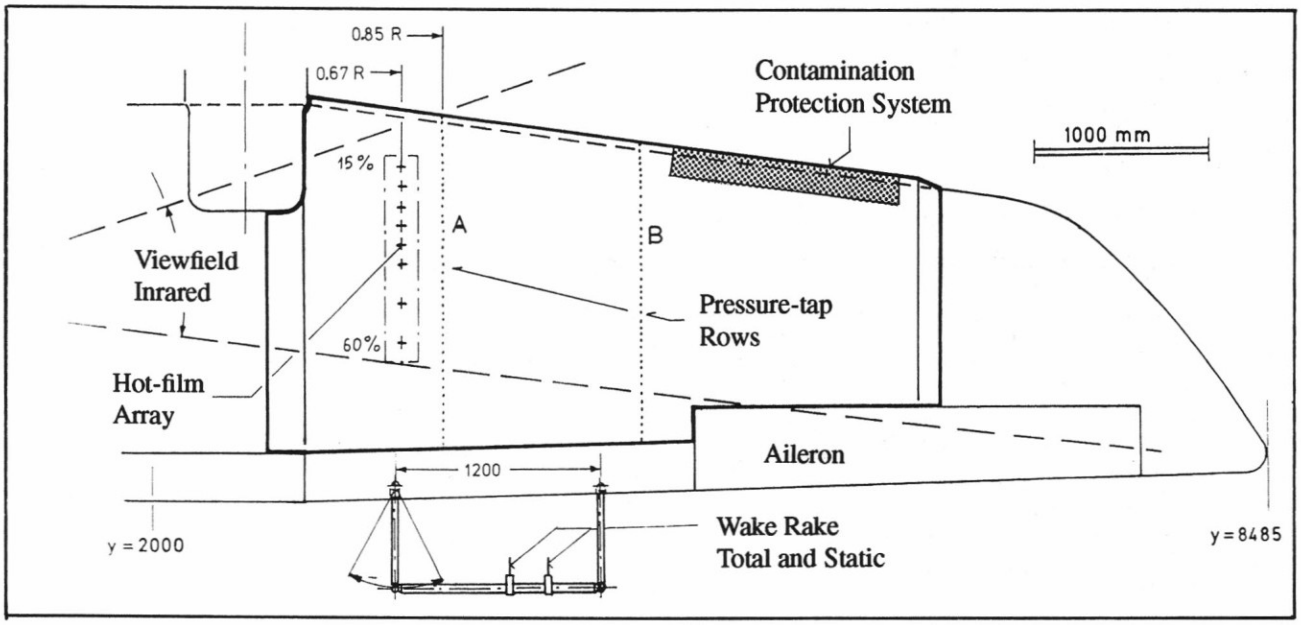

Fig. 7 Measuring equipment of laminar glove

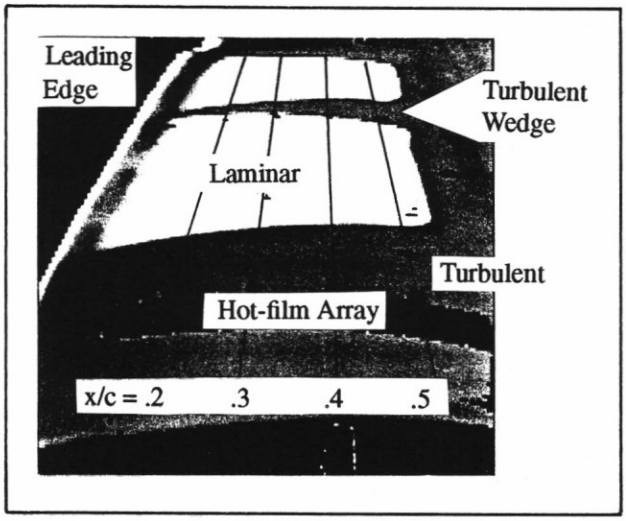

Fig. 8 Typical upper surface infrared image

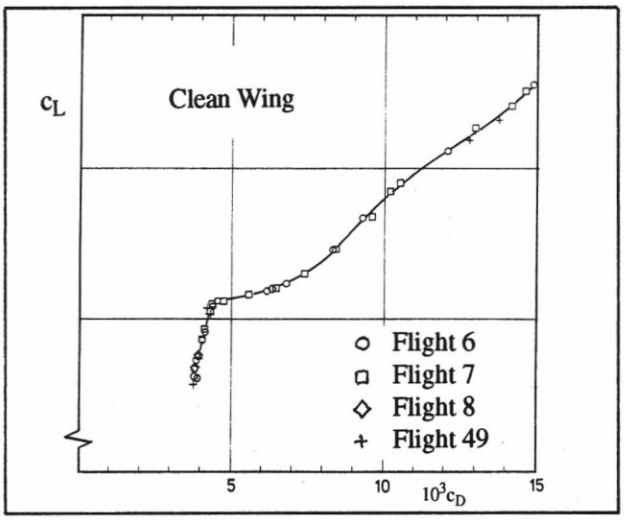

Fig. 9 Drag polar with natural transition

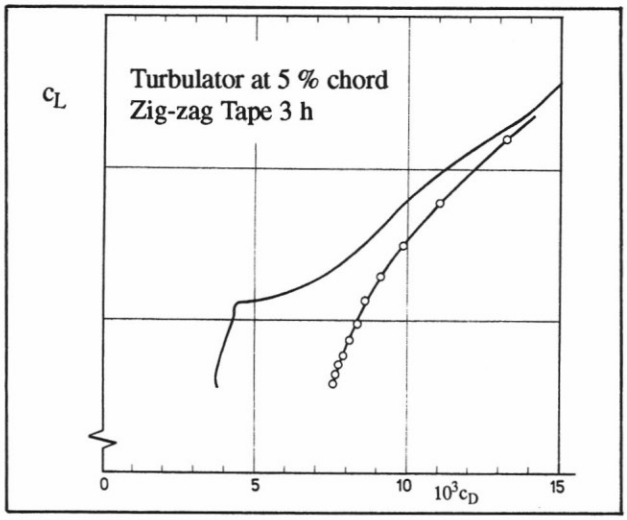

Fig. 10 Drag polar with fixed transition

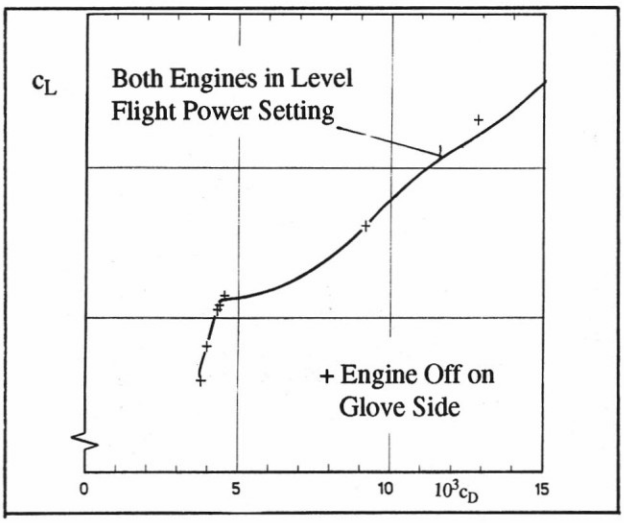

Fig.11 Influence of Engine Noise on the Drag Polar

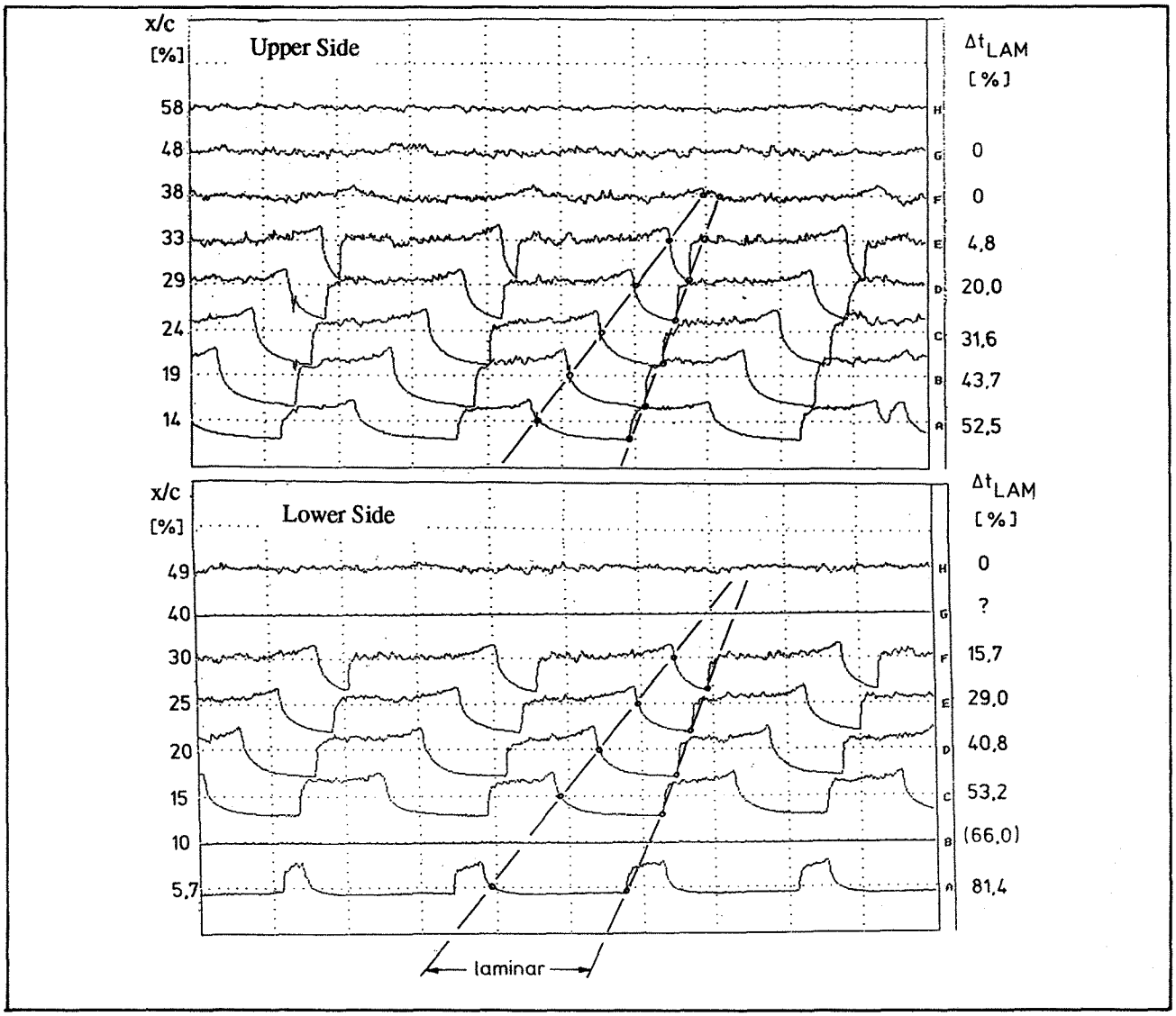

Fig. 12 Time histories of hot-films at different chord positions in the propeller slipstream

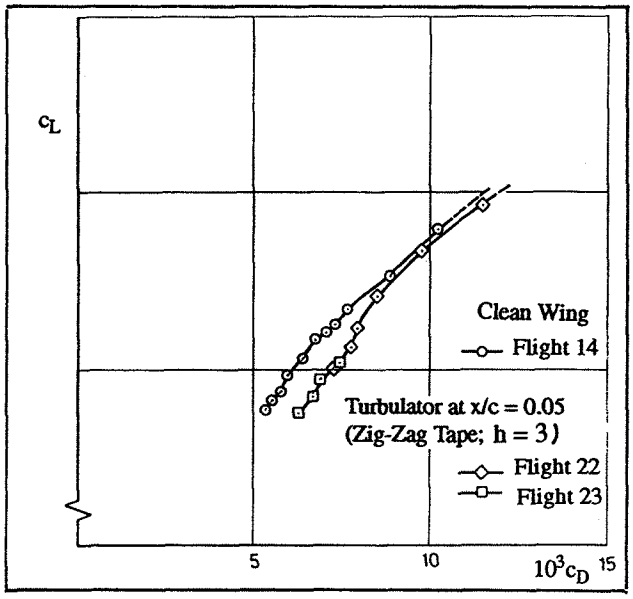

Fig. 13 Drag polars in the propeller slipstream

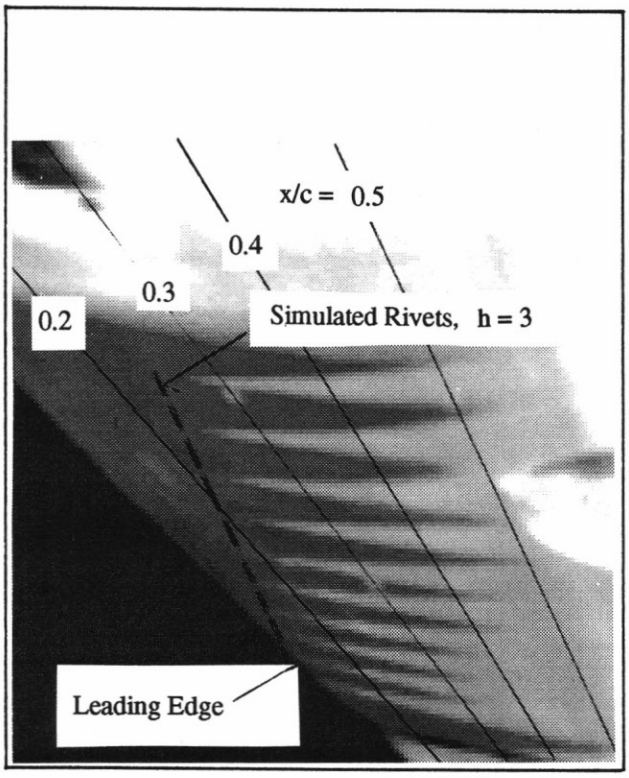

Fig. 14 Infrared image lower side with simulated rivets

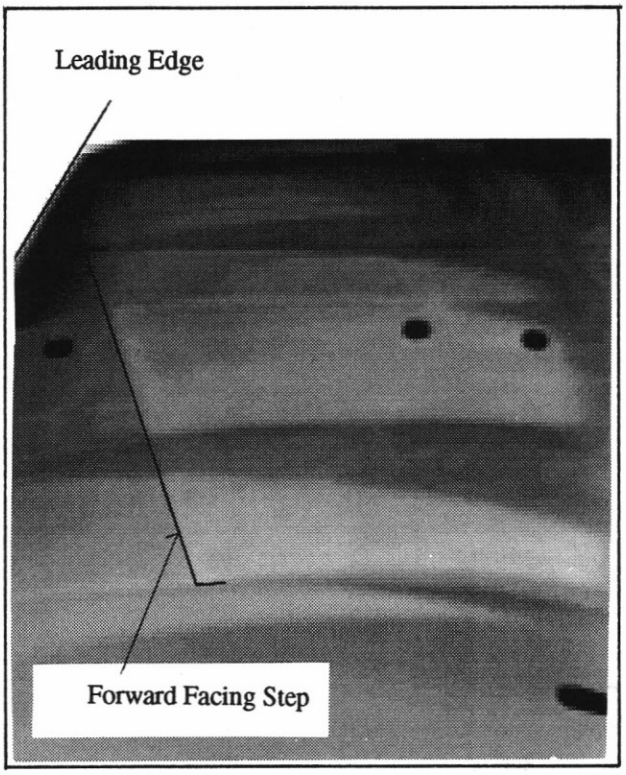

Fig. 16 Infrared image upper side with forward facing step

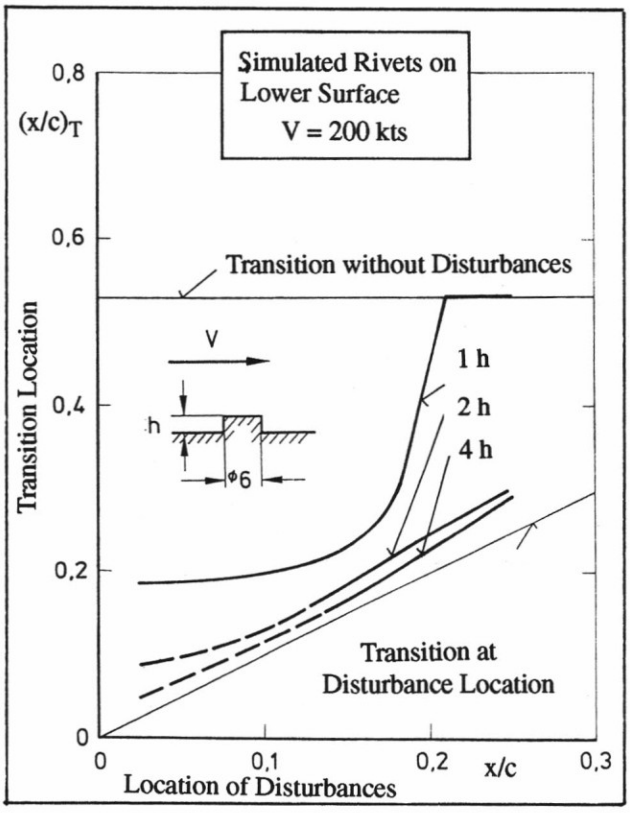

Fig. 15 Influence of simulated rivets on transition location

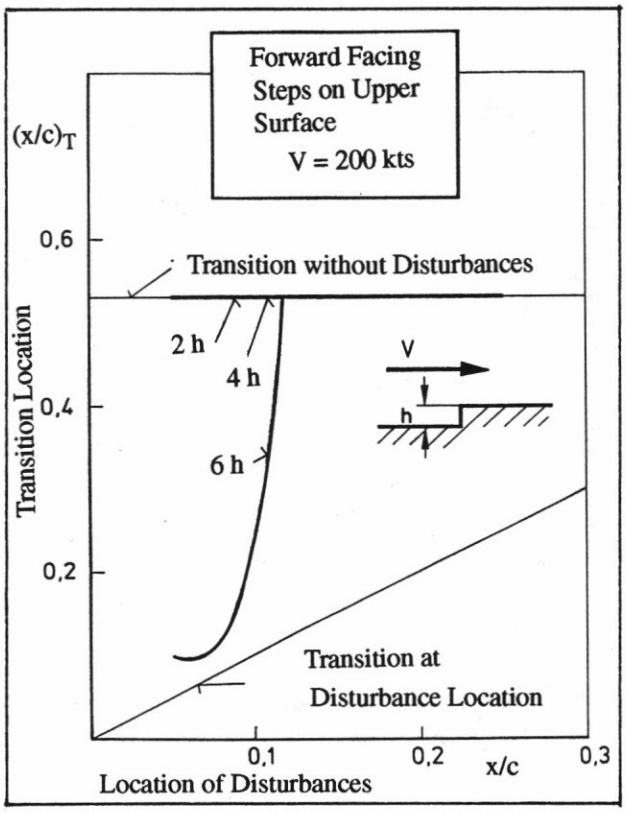

Fig. 17 Influence of forward facing steps on transition location

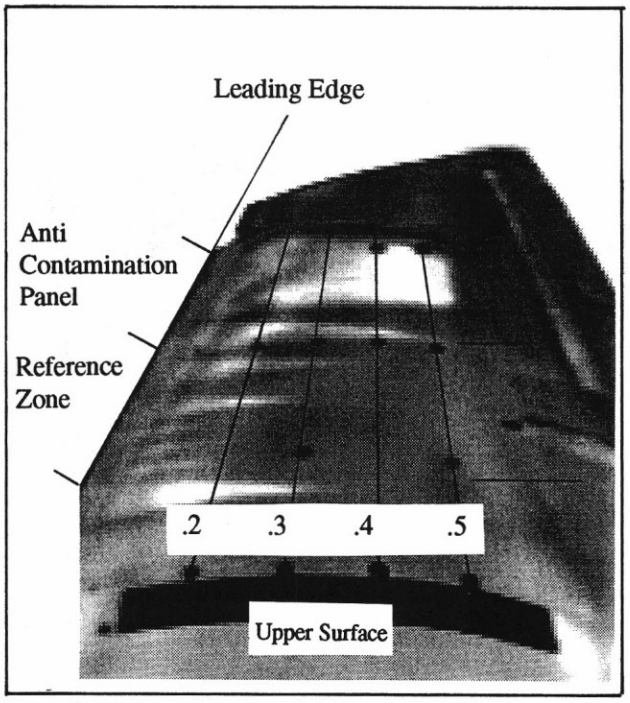

Fig. 18 Infrared image of the efficiency of anti-contamination system

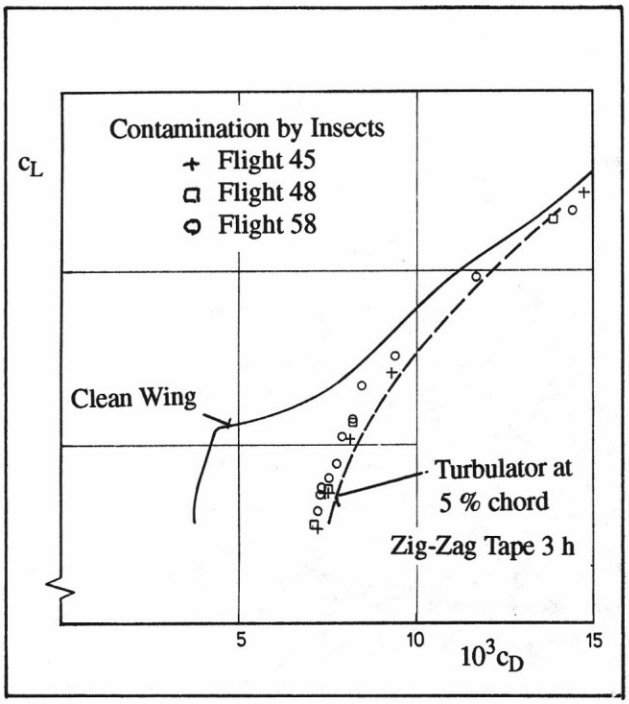

Fig. 19 Influence of insect contamination on the drag polar of the laminar glove

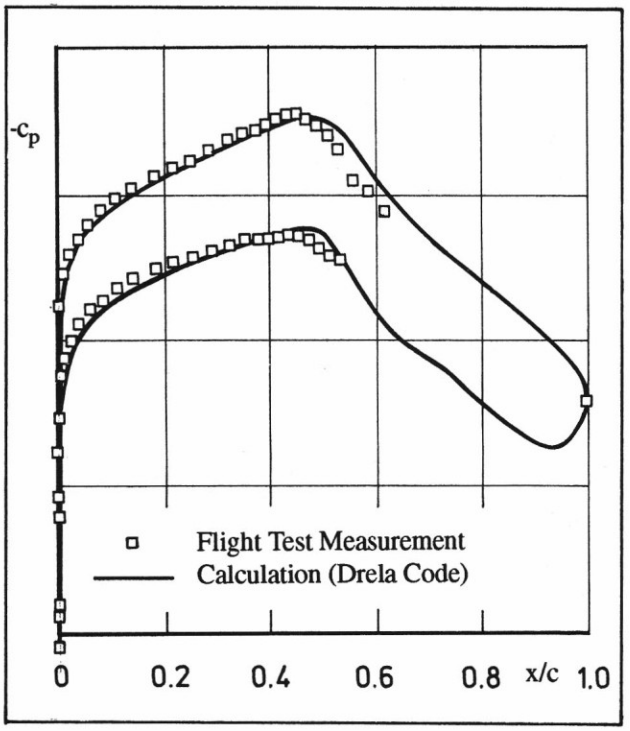

Fig. 20 Comparison calculated and measured pressure distribution of laminar profile

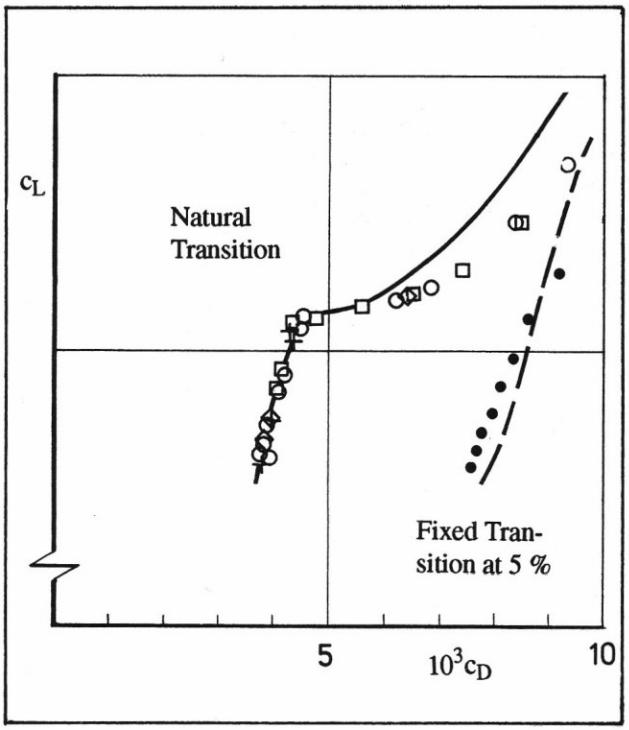

Fig. 21 Comparison of calculated and measured drag with natural and fixed transition